

Surface evolution of Ni–V transparent oxide films upon Li insertion reactions

R. Zanoni,¹ F. Decker,^{1*} C. Coluzza,² F. Artuso,^{1†} N. Cimino,¹ G. Di Santo² and E. Masetti³

¹ Dipartimento di Chimica and INFM, Università degli Studi di Roma 'La Sapienza', P. le A. Moro 5, I-00185 Rome, Italy

² Dipartimento di Fisica and INFM, Università degli Studi di Roma 'La Sapienza', P. le A. Moro 5, I-00185 Rome, Italy

³ ENEA-Casaccia, Thin Films Laboratory, Via Anguillarese, 00060 Rome, Italy

Received 17 May 2002; Revised 18 July 2002; Accepted 18 July 2002

A detailed picture is reported of the nature of an Li insertion Ni–V mixed-oxide electrode and of its evolution upon prolonged intercalation/deintercalation cycles. A combination of bulk and surface-sensitive techniques is used, including electrochemical analysis (cyclic voltammetry, impedance spectroscopy), atomic force microscopy (AFM) and XPS. The Ni–V oxide film, obtained by r.f. sputtering as a thin film on conductive glass for use as a transparent electrode in electrochromic windows, is an Li insertion material with high charge capacity, very good reversibility and a surface morphology characterized by a low initial roughness. Its surface composition shows an initial Ni enrichment. The nominal Ni–V stoichiometry is recovered already after ten cycles. Extended Li charge–discharge cycles induce progressive changes in the electrode reversibility (capacity fading) and in the reaction kinetics (increase of impedance). The surface evolution consists of the progressive accumulation of an Li carbonate layer, with thickness and roughness increasing with the number of cycles. The constancy of the core level and Auger peaks of Ni and V after 100 cycles excludes major changes in the electronic structure of the host oxide. However, electrochemical and AFM experiments performed after 1000 cycles indicate that the carbonate deposition on the electrode progresses further, therefore the surface layer is unable to yield a permanent electrode passivation and stabilization. Copyright © 2002 John Wiley & Sons, Ltd.

KEYWORDS: mixed oxides; Ni vanadates; intercalation; surface characterization; electrochemical properties; electrodes; electrochromism

1 INTRODUCTION

Transition-metal oxides are widely studied for rechargeable lithium batteries, in search for intercalation compounds with improved structural stability and good electrochemical performance. The same compounds have often been chosen in the form of powder for Li batteries, and of thin film as transparent electrodes for electrochromic devices (ECD), in order to act as host in the Li intercalation reaction. A peculiar feature of the vanadate-based materials is the flexibility and tunability of their electrochemical behaviour. According to their composition and crystal structure they can act as either anodes or cathodes with large specific capacity^{1,2} and many vanadates keep a low optical absorption in the visible range both in the charged and in the discharged state. This last property makes vanadates ideal candidates as optically passive counter-electrodes in ECDs with very high visible light transmittance.³

An important issue to be addressed for ECDs and rechargeable battery application is the electrode capacity fading over the first few cycles and the intercalation irreversibility over several hundreds or thousands of charge–discharge cycles, which would limit the lifetime of practical devices. With respect to this issue, a very important role in the device lifetime is played by the surface of active Li intercalation materials, because even small changes in surface properties can greatly affect the reaction kinetics. This is especially true for thin-film electrodes, for which there is a very high surface-to-volume ratio compared with that of other intercalation electrodes.

Basic electroanalytical characterization such as cyclic voltammetry (CV), chronopotentiometry or electrochemical impedance spectroscopy (EIS) can point out bulk processes (e.g. phase transitions or amorphization upon discharging,⁴ Li irreversible retention) and sometimes surface processes (e.g. electrode passivation or modification).⁵ To understand the complicated surface modifications of intercalation electrodes, several authors have resorted to spectroscopic measurements (FTIR, XPS)⁶ and to morphological analysis on the nanometre scale by atomic force microscopy (AFM)⁷ in conjunction with EIS.⁸ Photoelectron spectroscopy in particular is a powerful tool for the interpretation of electronic changes in Li intercalation materials being able to address selectively

*Correspondence to: F. Decker, Dipartimento di Chimica and INFM, Università degli Studi di Roma 'La Sapienza', P. le A. Moro 5, I-00185 Rome, Italy. E-mail: franco.decker@uniroma1.it

†Present address: ENEA-Palermo, Via Catania 2, 90141 Palermo, Italy.

Contract/grant sponsor: MURST; Contract/grant number: PRIN1999.

each constituent element prior to and after reaction. Relevant issues have been addressed on intercalated electrodes, by conventional or more recently synchrotron radiation-excited photoemission.^{9,10}

The versatility of XPS is exemplified in studies on the electronic structure of well-established electrochromic materials such as WO_3 ,¹¹ on *in situ* investigations on large-area electrode materials¹² and on the determination of the surface composition of reactive electrodes as a consequence of the use of different electrolytes or solutions.¹³

The aim of our paper is to monitor the evolution of some aspects of Li insertion reaction that are mostly relevant to the performance of an intercalation electrode. We have, in fact, followed the capacity fading and the surface passivation during the first hundreds of charge–discharge cycles by complementing the basic electrochemical techniques with the surface-specific methods of AFM and XPS. This complementary approach was considered to be important in the case presented here, where a new material based on mixed Ni–V oxides was developed in our laboratory that was very promising as an optically passive transparent electrode for ECDs with high charge capacity¹⁴ but is affected by a minor but significant and undesirable passivation effect.

The performance and lifetime of such thin-film oxides have been studied recently by means of several electrochemical techniques¹⁵ and was among the best recorded so far for this kind of film electrode: after 1000 cycles the fading of the charge capacity was less than 0.01%, when the inserted charge was still as large as 44 mC cm^{-2} . Nevertheless, the evolution of the film impedance, increasing with the number of charge–discharge cycles, was a matter of concern because it is an indication of a kinetic barrier growing up in time. Such modifications of the electrochemical behaviour were attributed to surface changes, and deserve further and detailed investigation with specific, sensitive experimental methods.

EXPERIMENTAL

Nickel–vanadium mixed-oxide thin films have been prepared by r.f. sputtering on substrates of ITO (indium tin oxide)-coated glass. The samples were obtained using a target made of cool-pressed powders of NiO (Cerac) and V_2O_5 (Cerac) mixed in an Ni/V atomic ratio of 1:4. The working pressure in the deposition chamber was 30 mTorr and argon and oxygen partial pressures were in the ratio of 5:1. The r.f. power applied was 200 W. Film thicknesses, measured by optical methods with a Perkin-Elmer $\lambda 9$ spectrophotometer, were found to be $\sim 110 \text{ nm}$. The morphology of the NiV-oxide layer, as revealed by AFM (VT-UHV AFM-STM by Omicron), was very homogeneous and flat in the scanning ranges of 5×5 , 2×2 and $1 \times 1 \mu\text{m}^2$, which is very similar to the morphology of the ITO substrate.

All electrochemical measurements were performed in three-electrode cells hermetically sealed under an argon atmosphere in a glove box. Lithium metal was used as counter- and reference electrodes whereas the working electrode was the thin-film oxide under investigation. The electrodes were immersed in a 1 M solution of lithium perchlorate in propylene carbonate. To promote Li insertion and

ageing of the electrode, CV and chronopotentiometry were accomplished between the potential limits of 1.0 and 4.5 V vs. Li/Li^+ , using an EG&G PAR 273 potentiostat/galvanostat. The CV curves were recorded after various cycles at a scan rate of 20 mV s^{-1} and the galvanostatic measurements were carried out at constant current densities of $\pm 50 \mu\text{A cm}^{-2}$.

A frequency response analyzer module, coupled with a potentiostat/galvanostat Ecochemie Autolab 12, was used to measure the complex electrode impedance, taking an a.c. modulation amplitude of 10 mV rms in the frequency range from 50 KHz to 1 mHz. A set of spectra was taken after ten voltammetric cycles. Each spectrum was recorded after a charge of 5 mC cm^{-2} has been injected at constant current ($I = 20 \mu\text{A cm}^{-2}$; $t = 250 \text{ s}$) and an open-circuit time of 20 000 s has been allowed to reach a steady state (a variation of $8 \times 10^{-7} \text{ V s}^{-1}$ has been recorded after this equilibration time). After the impedance measurements, the samples have been deintercalated up to a potential of 4.5 V vs. Li/Li^+ and allowed to relax at open circuit until they reach a stable V_{oc} value.

In order to follow the evolution of EIS spectra upon cycling, impedance measurements have been carried out on Ni–V samples after various CV cycles. All films have been cycled in the potential window of 1–4.5 V vs. Li/Li^+ , at a scan rate of 20 mV s^{-1} , and the EIS spectra have been recorded after complete deintercalation (4.5 V) of the samples and after an equilibration time of 7200 s. After EIS measurements, the sample held in either the intercalated or deintercalated state was withdrawn from the cell, washed in acetonitrile, dried and transferred under an argon atmosphere to the Omicron AFM, where most images of the deintercalated samples were taken in air. After that, the sample was returned to the electrochemical cell for further cycling. For a better reproducibility of the working conditions, as in a real device, the cell electrolyte was not changed between AFM measurements taken at the various cycles. To verify the homogeneity of the samples, four different areas were scanned, usually a few millimetres apart. The relevant quantity directly calculated from the images is the rms roughness, defined as the standard deviation of the pixel height.

The XPS measurements were conducted on Ni–V oxide samples as-prepared and after 10 and 100 intercalation/deintercalation cycles. In order to minimize charging under x-rays, the samples were mounted on conductive stubs by means of a small Cu spring pressed against the ITO conductive layer in the region used for contacting the electrodes. The as-prepared sample was stored in air after preparation, and measured as such. Special care was taken in order to avoid surface contamination of the treated samples and to prevent air exposure of the 10 and 100 cycle samples during their transport from the dry-box, where the intercalation/deintercalation cycles were performed, and the XPS instrument. Samples were treated electrochemically shortly before each XPS analysis, and transferred at the end of each electrochemical treatment in a vacuum-tight stainless-steel vessel preventively introduced in the Ar-filled dry-box and equipped with a transfer mechanism and an ultrahigh vacuum (UHV) valve. The vessel was then connected to its

dedicated flange on the XPS instrument, the dead volume was evacuated before opening both the vessel and the XPS preparation chamber valve, and the samples were eventually placed inside the holder in the XPS chamber. The XPS spectra were acquired with a VG Escalab Mk II spectrometer (CNR, Area della Ricerca di Roma, Montelibretti), equipped with a hemispherical analyzer operated in fixed analyzer transmission (FAT) mode with a pass energy of 20 eV. Unmonochromatized Al K α photons ($h\nu = 1486.6$ eV) were used to excite photoemission. The x-ray beam intensity was set to 280 W (14 kV \times 20 μ A) in order to obtain a good signal-to-noise ratio, particularly at the Li 1s core line. The binding energy (BE) scale was calibrated by taking the Au 4f $_{7/2}$ peak at 84.0 eV. In these conditions, Cu 2p $_{3/2}$ and Ag 3d $_{5/2}$ lines fall at 932.7 and 368.3 eV, respectively. All BEs are referenced to a value for the residual pump oil contamination-related C 1s peak taken at 285.0 eV. The spectra were collected by a μ -PDP 11/83 DEC computer and processed by means of VGS 5250-SI software (version of Feb. 1991). A series of commercially available DOS and Windows routines were used for data analysis. The accuracy of reported BEs is ± 0.2 eV and the reproducibility of the results is within these values. Atomic ratios for the as-prepared sample have been calculated from the ratio of the peak areas normalized by atomic cross-sections and corrected for an inverse dependence of the square root of kinetic energies. The contribution from the Ni 2p $_{3/2}$ shake-up satellite was added to the parent peak area. Atomic ratios are associated with an error of $\pm 10\%$. In the case of the deintercalated samples, where a carbonate overlayer is established, the same approach was used for the following reasons. The AFM images do not allow a confident estimate to be made of the relative fraction of exposed vs. covered Ni vanadate surface, because it does not allow for chemical assignment. Moreover, the height of the deposits seen by means of AFM is quite variable on the nanometre scale. In the absence of such crucial information, a decision was made not to introduce arbitrary corrections to the basic quantitation model, and to refer to future spectromicroscopic measurements with synchrotron radiation for a very accurate local quantitation.

RESULTS AND DISCUSSION

Cyclic voltammetry

Studies of the intercalation mechanism of lithium in Ni-V mixed-oxide thin films have been accomplished by simultaneous CV and EIS characterization. The electromotive force of the as-deposited thin films was found to be 3.5 V vs. Li/Li $^+$ immediately after cell assembling. The behaviour of r.f.-sputtered thin films of vanadium-nickel mixed oxides during CV has been investigated already by Lourenco *et al.*¹⁴ In order to reach a better resolution, a CV curve at the 10th cycle has been recorded at a slow scan rate of 1 mV s $^{-1}$ and is reported in Fig. 1(a). The sample showed an electrochemically active region between 1.5 and 3.5 V. Two well-distinguished cathodic peaks appear, whereas during the positive scan the oxidation peaks were less separated. Because the positions of these peaks are quite similar to

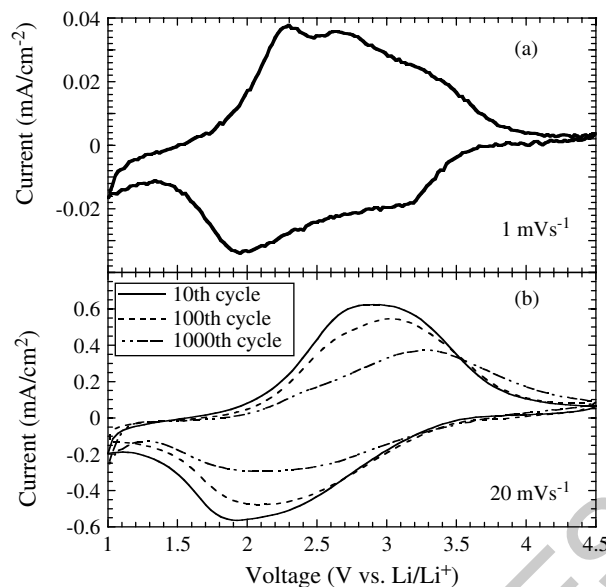


Figure 1. (a) Cyclic voltammogram (10th cycle) of Ni-V thin oxide film recorded at a scan rate of 1 mV s $^{-1}$. (b) Cyclic voltammetry curves recorded after 10, 100 and 1000 cycles at a scan rate of 20 mV s $^{-1}$.

those of V $_2$ O $_5$ reported in the literature,¹⁶ it could be supposed that only vanadium participates in the redox reaction and nickel is not electrochemically active during the intercalation/deintercalation process. This was confirmed by XPS analysis, which showed no evidence of nickel reduction due to lithium insertion.

In order to determine the stability of the film upon prolonged cycling, the CV curves after 10, 100 and 1000 cycles have been compared (Fig. 1(b)).

Most of the irreversible charge is retained permanently during the first cycle (18% of the charge inserted) but a capacity fading occurs also with prolonged electrode aging (the sample showed a capacity loss of 14% from the 10th to the 100th cycle and a further loss of 23% after 1000 cycles).

At the 10th cycle the charge capacity was as high as 40.7 mC cm $^{-2}$ (corresponding to an insertion level of 1 Li ion per V atom) for a CV at a scan rate of 20 mV s $^{-1}$, and the electrochemical process had good reversibility. Further cycling up to 100 CV scans led to a small loss of capacity down to 35.0 mC cm $^{-2}$. After 1000 cycles the intensity of the peaks decreased and the charge capacity dropped to 26.7 mC cm $^{-2}$. Moreover, the anodic peak was displaced to higher potentials with respect to the cathodic one (3.2 V). This behaviour can be attributed to a decrease of the ionic diffusion rate and to an increase of the electrode resistance, such as that of resistive layers grown on a passivated electrode surface. In fact the problem of the stability of Ni-V thin-film electrodes under cycling has been correlated to the presence of films formed on the surface of the active oxide when these electrodes are cycled between low and high potential limits in lithium salt non-aqueous solutions. The idea that the formation of surface deposits due to electrode-solution interactions occurs during intercalation/deintercalation cycles has been based also on extensive studies that included morphological and structural analysis (AFM, XPS) in conjunction with EIS.

Electrochemical impedance spectroscopy

Electrochemical impedance spectroscopy was used as a tool to investigate the film electrode intercalation kinetics and in particular for a better comprehension of surface phenomena occurring at the electrode/electrolyte solution interface. Our attention was mainly focused on the qualitative study of EIS spectral evolution upon intercalation and prolonged cycling. Figure 2 shows a series of impedance plots measured after ten charge–discharge cycles at different intercalation levels (corresponding to different potentials) in 1 M PC/LiClO₄ solution. Before recording each spectrum, a charge of 5 mC cm⁻² was injected and enough time to reach a steady state was allowed. The spectra are strongly potential dependent and clearly reflect the multistep nature of the overall lithium insertion process. Good separation of the relevant time constants was obtained. The first high-frequency semicircle does not depend on the intercalation level and probably reflects the involvement of an Li ion migration step through a thin layer on the electrode surface. The overall Li insertion into the vanadium-oxide includes a necessary step of Li ion migration through the surface layer that is initially formed. The high-frequency loop has been interpreted as the electrical response of this surface layer.¹⁷

The second arc, which clearly appeared only after an inserted charge of 25 mC cm⁻², can be ascribed to the charge-transfer resistance R_{ct} and to a double-layer capacitance C_{dl} at the interface between the surface films and the active oxide thin-film electrode. This second semicircle depends strongly on the potential (it becomes wider with potential lowering and consequently with lithium insertion), probably because of interfacial phenomena connected to the increase in Li ion concentration, or due to the more insulating character of this mixed vanadium oxide with a larger intercalated charge. This enlargement, however, is reversible (the semicircle

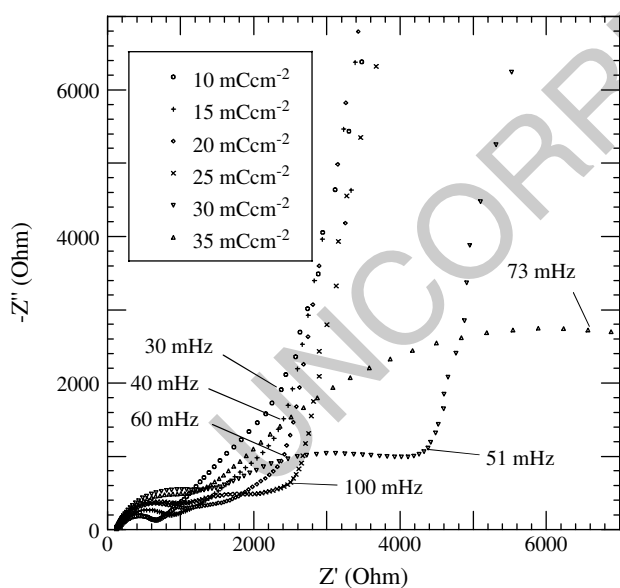


Figure 2. The EIS spectra (50 kHz–1 mHz) of Ni–V thin oxide film recorded after 10 charge–discharge CV cycles at different intercalation levels (inserted charge from 10 mC cm⁻² to 35 mC cm⁻²).

appeared to contract upon deintercalation), as evidenced by EIS measurements taken after lithium deinsertion.

Referring to the work of Shibuya *et al.* on Li_xCoO₂¹⁸ we can speculate that the increase of the charge-transfer resistance with the intercalation level can be connected with a decrease of the electronic conductivity of the film.

The time constant of the charge-transfer process merges with that related to the semi-infinite solid-state diffusion of lithium inside the film, which is usually represented in the impedance spectrum as a straight line at ~45° in the medium-frequency range. At low frequency the spectra are characterized by an almost vertical line that is typical of intercalation electrodes in the form of thin films deposited on electronic conductors impermeable to Li ions. This part of the spectrum is determined by the ion accumulation in the finite volume of the thin film. The slope slightly below 90° was explained by other authors¹⁹ as being due to the roughness at the blocking electrode/electronic conductor interface in the case of porous films.

The effect of repeated intercalation/deintercalation cycles on the electrochemical performances of the Ni–V thin-film electrodes has been investigated and the results are reported in Fig. 3. The series of spectra clearly shows that upon cycling the high-frequency semicircle became gradually larger, indicating both a thickening of the surface passivating layers and an increase of the charge-transfer resistance. The formation of surface deposits under electrode aging has been discussed extensively by Aurbach *et al.* in different works aimed to investigate the interactions between electrode materials for lithium batteries (graphite, Li_xCoO₂, Li_xNiO₂, Li_xMn₂O₄, etc.) and non-aqueous lithium salt solutions.^{8,15,20} They also suggested a model for fitting the EIS spectra, including a Randles circuit in series with a Voigt-type analogue (several elements in series, constituted by a resistance and a capacitance in parallel) and reflecting the Li ion migration through the multilayer surface films.

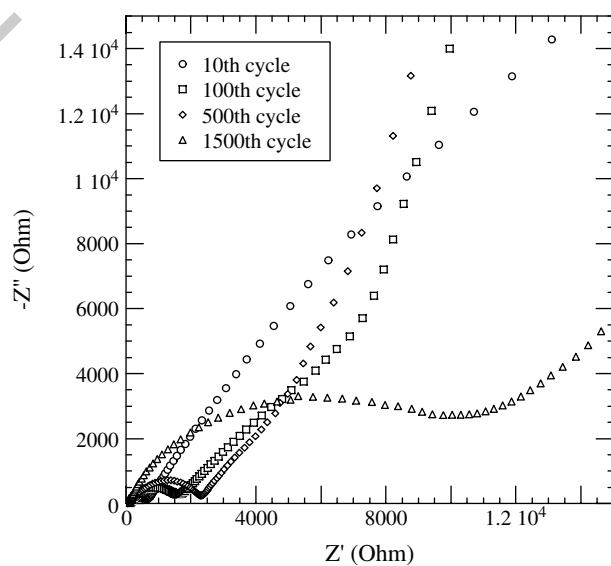


Figure 3. Evolution of impedance spectra (sample as in Fig. 2) as a function of cycling. Spectra were taken, always in the deintercalated state, from the highest to the lowest frequency (50 kHz–1 mHz).

1 The same model has been applied by us in a previous work
2 on the Li intercalation kinetic studies of r.f.-sputtered Ni–V
3 thin film.¹⁵ As will be discussed the next section *ex situ*
4 AFM measurements confirmed that after repeated long cycle
5 operation the electrodes become more extensively covered
6 by a surface film: the nature of this surface layer has been
7 investigated further by XPS measurements.

8 Atomic force microscopy

9 The value of the real surface area is a very important param-
10 eter to estimate the electrochemical activity of deposited films.
11 In order to evaluate it, we performed AFM measurements
12 on samples treated differently. We measured samples inter-
13 calated and deintercalated from 10 to 1500 times. Following
14 the electrochemical cycling, analysis of the images revealed
15 three main morphological changes in the surface structure of
16 the samples.
17
18

19 The morphology of the as-deposited sample surface
20 showed a well-ordered array of round-shaped grainslike
21 the homogeneous ITO substrate on which the film has
22 been grown. The grain mean lateral size is 50–100 nm,
23 with an average height of ~20 nm. These samples showed a
24 roughness (6 ± 2 nm) comparable with that of the substrate
25 (see Fig. 4(a)). This could be explained by assuming that
26 the growth has been ordered on it, transferring on the film
27 surface the substrate morphology. The result indicated that
28 the films were homogeneous and the real surface was just
29 10% greater than the geometrical one (i.e. the surface can
30 be assumed to be totally planar). The first visible effect of
31 the cycling (Fig. 5(a)) was the unexpected formation of some
32 bidimensional structures (whiskers or polymeric ribbons)
33 on the surface of the sample. The formation of those structures
34 was typically seen after 10–20 cycles. Those structures were
35 up to 4 μm long, 100 nm wide and 100 nm high. On the
36

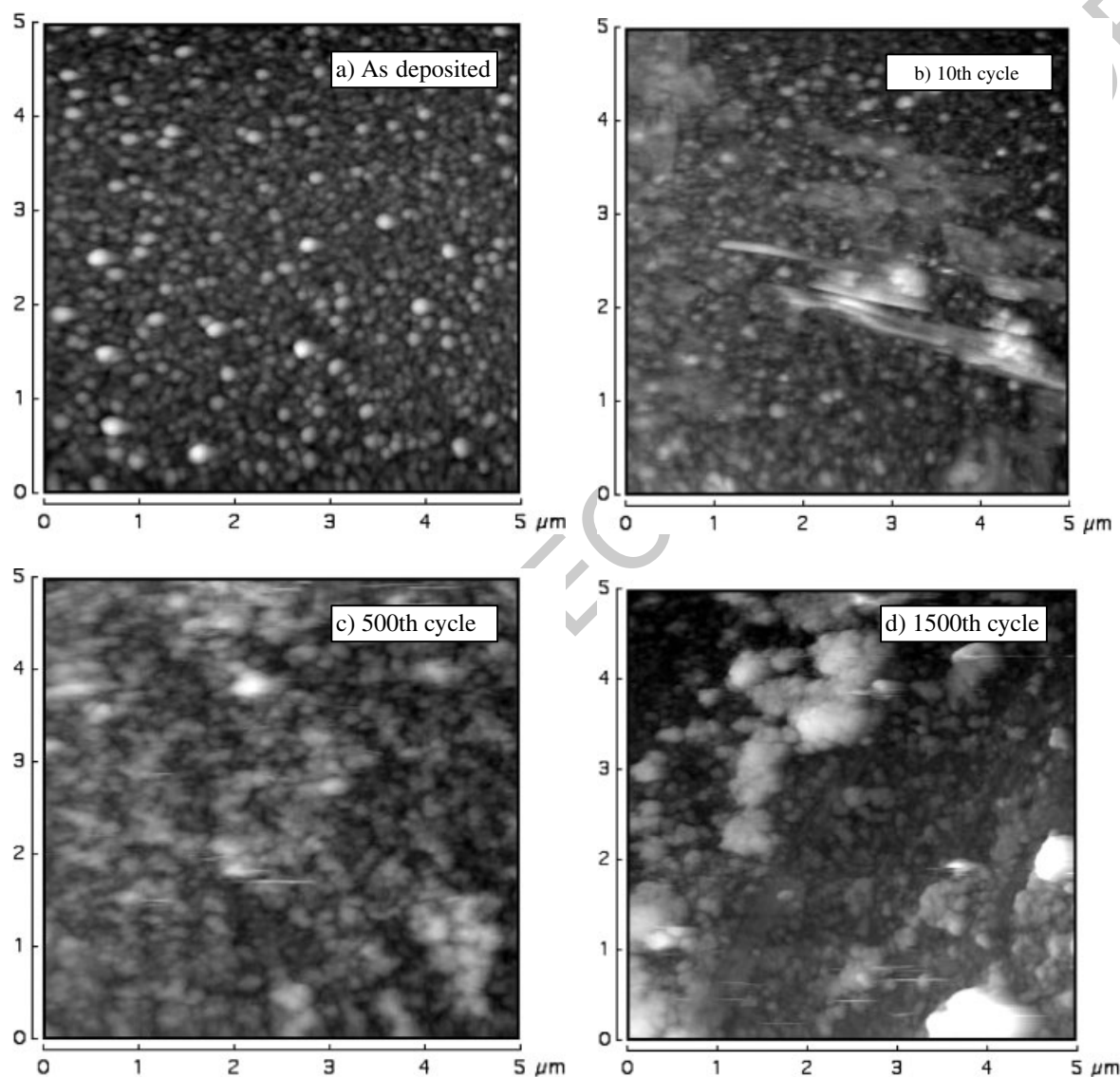


Figure 4. The $5 \times 5 \mu\text{m}^2$ AFM images of Ni–V mixed-oxide thin film as-deposited (a) and deintercalated (b–d) after CV cycles. The image of the as-deposited sample (a) shows a regular and ordered array of round-shaped grains with a roughness value of ~6 nm. After 10 cycles the image shows a partial coverage of the as-deposited surface (b). In this case an increase of the mean grain lateral size and roughness (~9 nm) can be seen. When the number of cycles goes to 500 (c) and 1500 (d), the round-shaped structures tend to cover the whole surface. A simultaneous increase of the roughness can be seen: 40 nm after 1500 cycles (see Fig. 6).

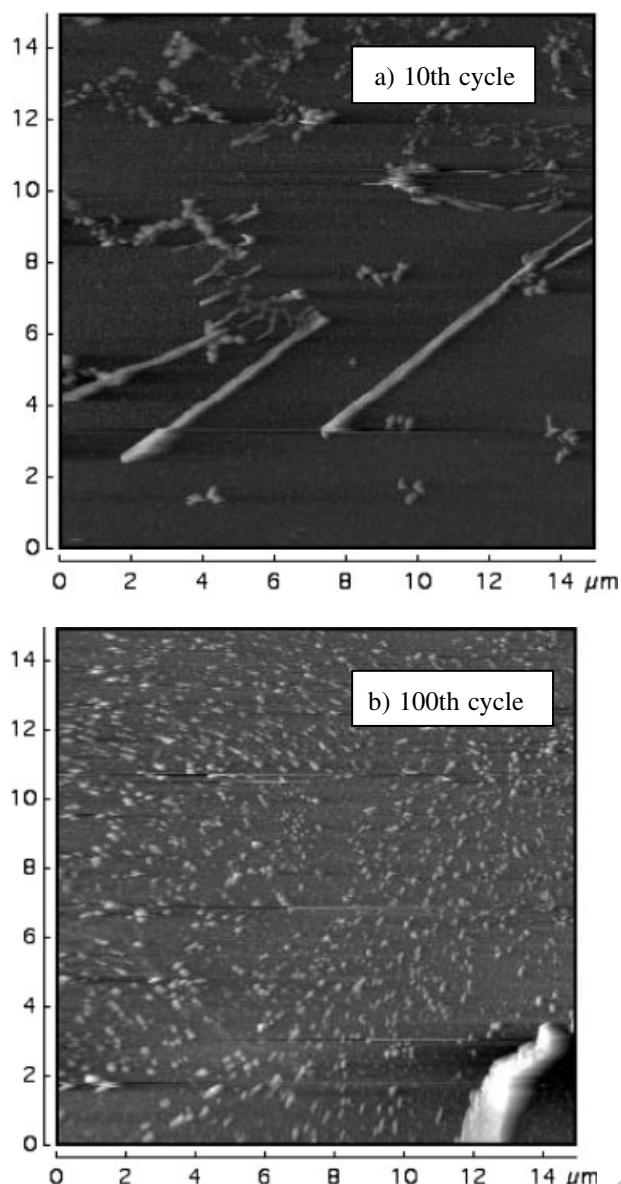


Figure 5. The $15 \times 15 \mu\text{m}^2$ AFM images of Ni–V mixed-oxide thin films after 10 (a) and 100 (b) CV cycles. At this frame size it is possible to observe the formation of some ‘stripe-shaped’ structures up to $4 \mu\text{m}$ long. After 100 cycles, these structures cover the surface more homogeneously than for a lower number of cycles. They become small, disordered and round shaped.

scanned areas where those structures did not cover the deposited film, we observed an Ni–V oxide layer not much different from the as-deposited surface (Fig. 4(b)). Software calculation of rms roughness give a value of $9 \pm 2 \text{ nm}$ and the calculated area of the real surface was 12% greater than that of the geometrical one. Such roughness is comparable, if not equal, to that of the pristine films.

After 500 cycles the bidimensional structures disappeared and the surface morphology became different (see Fig. 4(c)) due to the formation of round-shaped cluster of flakes deposited all over the sample. The mean lateral grain size increased up to 200–300 nm. The roughness reached a value of $25 \pm 4 \text{ nm}$ and the real surface area was 20% greater than

the geometrical one. After 1500 cycles (Fig. 4(d)) the surface morphology was different from one sample to another. Some samples showed very large grains (1000 nm), whereas, others presented much smaller grains (400–500 nm). Both types of samples showed a quite similar mean rms roughness of $\sim 40 \text{ nm}$ and a real surface area 30% greater than the geometrical one.

Images $15 \times 15 \mu\text{m}^2$ after 10 (Fig. 5(a)) and 100 (Fig. 5(b)) CV cycles can give an idea of what happens on the surface after a few cycles. On a large scale, the formation of some ‘stripe-shaped’ structures can be seen. After 100 cycles, these structures cover the surface more regularly than before, becoming small, disordered and round shaped.

As mentioned before, we assumed that the rms roughness—related to the real surface area value—was the meaningful parameter. A plot of the roughness vs. cycle number showed a monotonic slope that confirmed roughening of the surface sample with increasing cycling, as can be seen in Fig. 6.

X-ray photoelectron spectroscopy

The XPS investigation was concentrated on characterization of the surface effects induced by the intercalation/deintercalation process after 10 and 100 cycles, i.e. when the surface structures evidenced by AFM are supposedly at their onset. The electronic structure of the as-prepared sample, both in terms of BE and of surface composition, was explored and compared with the cycled samples.

In the investigated series, the Ni 2p ionization spectrum is invariably composed of a main ionization peak falling in the narrow range 856.5–856.7 eV plus shake-up satellites due to the excitation of an Ni 3d electron into an unoccupied Ni orbital concurrently with the emission of photoelectrons (Fig. 7). The presence of shake-up satellites is characteristic of Ni(II) paramagnetic species in octahedral and tetrahedral coordination, as reported in early literature findings,²¹ where it has been shown that the satellite number, intensity and energy separation from main peaks are variable to a large extent in different species. Based on the phase diagram of the NiO–V₂O₅ system²² and on the experimental conditions for sample production adopted here, the present sample composition could be expected to be a mixture of Ni(VO₃)₂

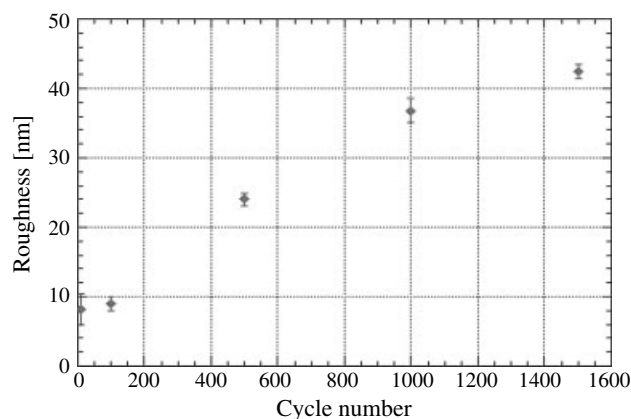


Figure 6. A plot of the mean surface roughness vs. the number of CV cycles. A monotonic increase of the roughness value with the cycling number is shown on the graph.

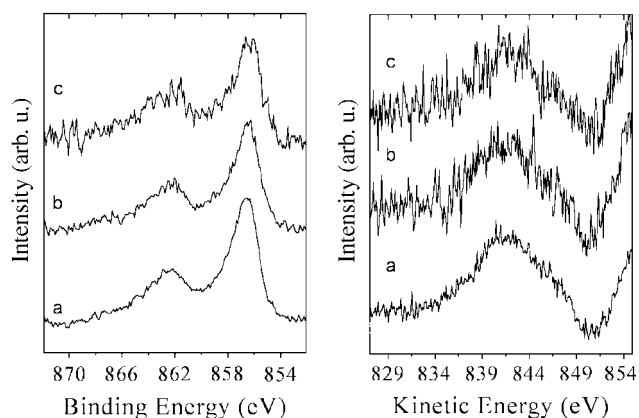


Figure 7. The Ni 2p ionization region (left panel), with the 3/2 spin-orbit component and the shake-up satellite line, and the Ni $L_{3M_{4.5}M_{4.5}}$ Auger spectra (right panel) for the Ni–V oxide samples: as-prepared (a); after 10 intercalation/deintercalation cycles (b); after 100 intercalation/deintercalation cycles (c).

and V_2O_5 . V_2O_5 has been characterized thoroughly by photoemission in several publications. In previous reports on related Ce vanadate samples,^{9,23} the V $2p_{3/2}$ BEs for vanadate and V_2O_5 were shown to fall in a very narrow energy range (517.45 and 517.545, respectively). This is further confirmed in Table 1, from a comparison with V $2p_{3/2}$ BEs from well-characterized $InVO_4$ and V_2O_5 oxides, both obtained as films on conductive substrates from a sol–gel route.²⁴

Among the known Ni vanadate compounds— $Ni(VO_3)_2$, $Ni_2V_2O_7$ and $Ni_3(VO_4)_2$ —the only species previously investigated by XPS is, to our knowledge, $Ni_2V_2O_7$ from Ni and V powders, used as an Li battery electrode material.²⁵ The paper contains no further reference to previous reports on strictly analogous systems and it lacks indications on the BE referencing procedures adopted there. Thus absolute XPS BEs cannot be compared with the present case, and a comparison is restricted to a discussion of lineshapes and BE separations. The Ni 2p lineshape in $Ni_2V_2O_7$ is close to those

from the mixed oxides reported here but the energy separation between V $2p_{3/2}$ and Ni $2p_{3/2}$ is 0.45 eV lower. In the absence of reference XPS spectra, the comparison can be extended to literature reports on Ni oxides/hydroxides and related compounds. Although the lineshape of Ni 2p is close to that of Ni hydroxide and definitely far from the well-known composite shape of the 3/2 component in NiO ,²⁶ its BE is distinctly higher than in $Ni(OH)_2$ (0.9–1.1 eV²⁶; 0.6–0.8²⁷; 0.4–0.6²⁸). Neither assignment, therefore, fits the data in the present case. The lineshapes and energy positions of either Ni 2p or Ni $L_{3M_{4.5}M_{4.5}}$ Auger peaks closely match in the series, as shown in Fig. 7 and by the data in Table 1. This clearly indicates that the initial electronic state of Ni is preserved through 100 cycles. It can be useful to recall here that for an atomic element the sum over the BE of a core line and the kinetic energy (KE) of an Auger is independent of the actual choice of a reference line for charging compensation, the two energy scales (BE and KE) being affected to the same extent and opposite in sign by any particular choice. The sum is termed the Auger parameter.²⁹

It is remarkable that the constancy in Ni 2p features (and, vide infra, in V 2p) occurs but a sizeable variation is shown in the Ni/V atomic ratio across the sequence of as prepared or 100 cycles. The values reveal an initial surface enrichment in Ni, whereas the nominal 1 : 4 ratio is reached after 10 cycles and is maintained after 100 cycles. The nominal stoichiometry would produce O/V and O/Ni atomic ratios of 2.7 and 11.0, respectively. The 10-cycle sample results in the composition closest to the nominal in the series, as deduced from the data in Table 2 (2.6, 8.9).

A comparable constancy along the intercalation cycles is shown by vanadium, as can be inferred from the values of V $2p_{3/2}$ BE and full width at half-maximum (see Fig. 8). Either set of values is fully compatible with a V^{5+} oxidic species, with no trace of V^{4+} .

The Ni–V electronic structure of the as-prepared Ni-doped V_2O_5 sample is largely recovered in the fully deintercalated investigated samples. The result is also

Table 1. The XPS binding energy values (eV), with full widths at half-maximum (eV), reported in parentheses.^a

	C 1s				O 1s		V $2p_{3/2}$	Ni $2p_{3/2}$	Li 1s
As-prepared	285.0 (1.6)	286.4 (2.3)	288.9 (1.8)	—	530.6 (1.6)	531.9 (2.5)	517.6 (1.7)	856.7 (3.1)	—
10 cycles	285.0 (1.6)	286.4 (2.3)	288.9 (1.8)	290.2 (1.6)	530.7 (1.6)	532.2 (2.0)	517.8 (1.8)	856.5 (3.1)	55.5 (2.0)
100 cycles	285.0 (1.6)	286.4 (2.3)	288.9 (1.8)	290.3 (1.6)	530.6 (1.6)	532.2 (1.8)	517.8 (1.8)	856.5 (2.9)	55.6 (1.8)
$Li_2CO_3^a$	285.0 (1.9)	286.6 (1.6)	288.9 (2.3)	290.3 (1.7)	—	532.2 (2.0)	—	—	55.4 (2.0)
$V_2O_5^b$	285.0 (1.6)	286.6 (1.6)	288.8 (2.0)	—	530.6 (1.6)	532.4 (2.5)	517.7 (1.4)	—	—
$InVO_4^b$	285.0 (1.8)	287.0 (1.8)	289.5 (1.8)	—	530.6 (1.6)	532.7 (2.5)	517.6 (1.6)	—	—

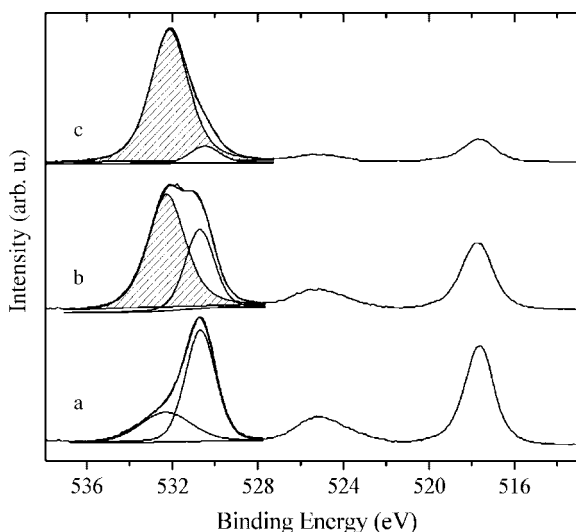
^a Li_2CO_3 is a commercial high-purity powder sample from Merck.

^b Both V_2O_5 and $InVO_4$ are reference samples obtained from sol–gel procedures as thin films on conductive glasses by Orel and Surca.²⁴ Their composition and structure were preventively investigated by chemical analysis and x-ray diffraction measurements.

Table 2. The XPS atomic ratios ($\pm 10\%$) for the reported samples.^a

	V/ Ni	O _{ox} / V	Li/ V	Li/ C _{CO₃}	O _{CO₃} / O _{ox}	O _{CO₃} / C _{CO₃}
As-prepared	2.5	2.8	—	—	—	—
10 cycles	3.4	2.6	3.3	3.0	1.8	4.2
100 cycles	3.5	1.8	11.2	2.5	9.2	3.6

^a Component O_{ox} is assigned to the metal oxide in the O 1s composite peak and O_{CO₃} and C_{CO₃} are assigned to carbonate in the O 1s and C 1s peaks, respectively. The ratios are obtained from V 2p_{3/2}, Ni 2p_{3/2}, Li 1s, O 1s and C 1s ionization peak intensities, using the procedure described in the Experimental section.

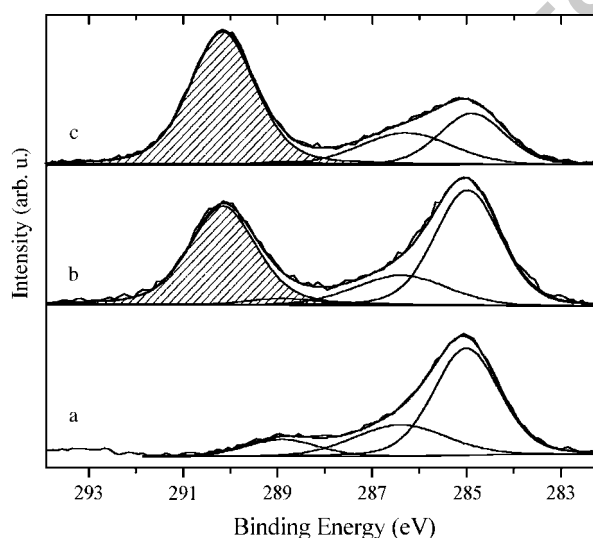
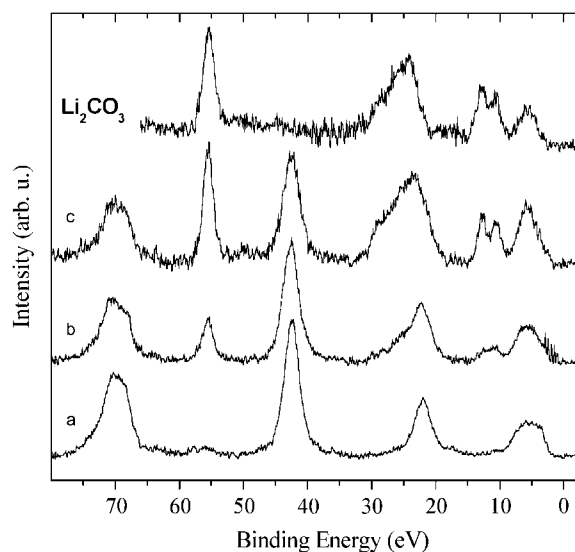
**Figure 8.** Extended region of the V 2p and O 1s ionization peaks for the Ni-V oxide sample. Labels (a)–(c) are as in Fig. 7. The carbonate-related component is as a hatched area.

1 consistent with our recent XPS experimental findings on
2 In-V₂O₅ analogous species, in which V recovered to its V³⁺
3 original state upon deintercalation, after conversion into V⁴⁺
4 upon Li⁺ intercalation.³⁰

5 The most striking effect of cycling is already evident
6 after 10 cycles and is definitely confirmed after 100: in
7 the O 1s and C 1s regions, a new component grows and
8 the valence band is thoroughly modified (Figs 8 and 9).
9 The BEs associated with the O 1s and C 1s components
10 coincide with the values for Li₂CO₃ (see Table 1) and
11 allow for an assignment of the new features to surface
12 carbonate. The assignment is independently and definitely
13 confirmed by the valence band spectra reported in Fig. 10.
14 In Fig. 10 the characteristic ionization peaks for Li₂CO₃,
15 which have been assigned to the various antibonding,
16 non-bonding and bonding combinations of oxygen- and
17 carbon-derived molecular orbitals in the carbonate ion,³¹
18 are in a 1:1 correspondence with the first four peaks in
19 the spectrum of the 100-cycle sample and can be easily
20 guessed in the 10-cycle sample too. A striking similarity
21 is shown between the Li₂CO₃ XPS valence bond and the
22 difference spectrum (100-cycle minus as-prepared sample,
23
24
25
26
27

normalized to the V 3p height) displayed in Fig. 11. Further
independent confirmation for the growth of a surface deposit
of Li₂CO₃ comes from the relative quantitative measurements
in Table 2, where a value of $2.5 \pm 10\%$ for the ratio of Li to
the carbonate-related C 1s peak was found after 100 cycles.
Although the formation of surface carbonate deposits has
been reported or speculated on (in some cases with the help
of XPS findings), in the case of Li electrodes and mixed-oxide
intercalation in organic carbonates³² the present results allow
the nature of the surface layer to be assigned to Li carbonate
only (within the sensitivity of the method) when propylene
carbonate is the electrolyte.

Remarkable excess in the Li/C_{CO₃} ratio, with respect to
the expected Li₂CO₃ stoichiometry, is found after 10 and 100
cycles, compatible with Li ion trapping on the oxide surface
or inside the film.

**Figure 9.** The C 1s photoemission region for the Ni-V oxide sample. Labels (a)–(c) are as in Fig. 7. The carbonate-related component is marked as a hatched area.**Figure 10.** Valence band photoemission spectra for the Ni-V oxide sample, including V 3p, Li 1s and V 3s + Ni 3p core peaks. Labels (a)–(c) are as in Fig. 7.

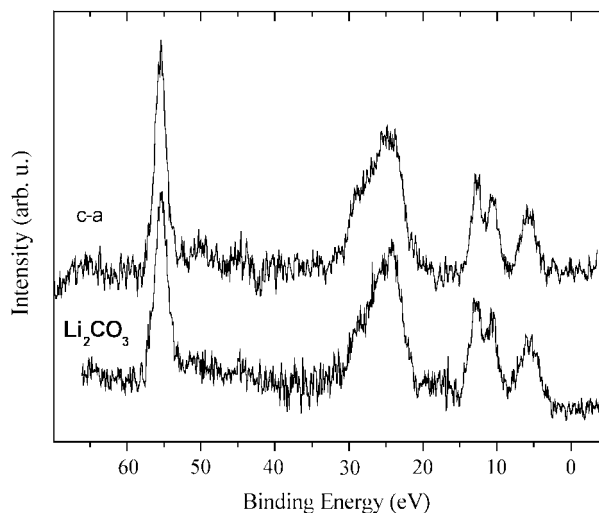


Figure 11. Valence band difference spectrum between samples (c) and (a) in Fig. 10. The two spectra have been normalized to the intensity of the V 3p core line. The corresponding spectrum from a powder sample of Li_2CO_3 is included for comparison.

As to the morphology of the surface layer, XPS data are compatible with a discontinuous deposit, suggested by AFM images, because Ni and V core lines are clearly visible even after 100 cycles, when the $\text{O}_{\text{CO}_3}/\text{O}_{\text{oxide}}$ atomic ratio is as high as 9.5. If a continuous layer were to be formed, its thickness should be smaller than the escape depth for Ni 2p photoelectrons in Ni(II) oxide/hydroxide, estimated as 2.4 nm.³³

CONCLUSIONS

The Ni–V sputtered oxides studied in this paper behave as efficient and almost reversible Li insertion transparent electrodes for several hundred charge–discharge cycles. The initial film composition, for which the Ni–V–O phase diagram suggests a 1:1 mixture of $\text{Ni}(\text{VO}_3)_2$ and V_2O_5 oxides, results in a slight surface enrichment of Ni.

The AFM images show uniform morphology of the pristine films with a low surface roughness (6 ± 2 nm). The AFM images and XPS spectra of the electrodes used were compared with those of the pristine sample after completing multiple Li electrochemical insertion–deinsertion experiments, followed by EIS. Activation of the full insertion capacity of these films, typically requiring 2–5 voltammetric cycles and the permanent retention of 1/5 of the total reversible charge, did not significantly change the overall film morphology, apart from the appearance of sparse crystals of elongated shape on isolated spots of the electrodes. The top surface layer contains some Li carbonate already after the 10th cycle, according to XPS results, and responds (at high modulation frequencies) as an Li-permeable, potential-independent RC• analogue in EIS. The excess in the Li/ C_{CO_3} ratio, with respect to the expected Li_2CO_3 stoichiometry, is compatible with the trapping of Li ions on the surface or inside the film, as suggested by the charge measurements during the first cycles.

After extended electrochemical cycling a consistent thickening of the Li carbonate deposit is detected by an increase of the corresponding photoelectronic signals and by the higher roughness from AFM. The EIS high-frequency measurements (100 and 500 cycles) show an increase of the impedance attributed to the Li-permeable surface layer, whereas some charge capacity fading is evidenced by CV. The XPS difference spectra (spectrum of the sample cycled 100 times minus the spectrum of the pristine sample) in the valence band region, besides confirming the exact correspondence of the signal from the surface layer of the cycled sample with that of the Li_2CO_3 standard, does not show any other passivating layer resulting from reaction of the organic solvent with the oxide film. The constancy of the core level and Auger peaks of Ni and V in the spectra of the treated electrodes excludes important changes in the electronic structure of the host oxide, which might have occurred via the multiple Li insertion/deinsertion reactions.

The CV, EIS and AFM experiments performed after 1000 cycles indicate, however, that the carbonate deposition on the electrode progresses further and that a true surface passivation and stabilization cannot yet be attained.

The surface characterization by AFM and XPS shown above, in conjunction with the electrochemical methods, provide a detailed description of several aspects of the Li insertion reaction during activation and extended cycle life tests of thin-film Ni–V oxide electrodes. These experiments suggest that the same experimental methods are suitable for analysis of a whole class of insertion reactions in thin-film electrodes with different compositions from various organic solvents.

A further improvement of this integrated approach will consist of surface chemical–topographic analysis with lateral submicron resolution of electrodes, presenting a peculiar morphology and/or structured reaction products at their interface. Such analysis is now under way by means of photoelectron spectromicroscopy, a tool now available with synchrotron radiation sources.

Acknowledgements

This work has been funded by MURST-PRIN 1999. The authors would like to acknowledge Dr. A. Lourenco, Physics Department, University of Campinas, Sao Paulo (Brazil), for the preparation of Ni–V mixed-oxide samples and Professor B. Orel and Dr. A. Surca, National Chemical Institute, Ljubljana (Slovenia), for the preparation of InVO_4 and V_2O_5 films used as references for XPS assignment.

REFERENCES

- Guyomard D, Sigala C, La Salle ALG, Piffard SY. *J. Power Sources* 1997; **68**: 692.
- Julien C. *Ionics* 2000; **6**: 30.
- Artuso F, Decker F, Krasilnikova A, Liberatore M, Lourenco A, Masetti E, Pennisi A, Simone F. *Chem. Mater.* 2002; **14**: 636; Varsano F, Croce F, Decker F, Masetti E. *Electrochim. Acta* 2001; **46**: 2069; Artuso F, Picardi G, Bonino F, Decker F, Bencic S, Šurca Vuk A, Opara-Krasovec U, Orel B. *Electrochim. Acta* 2001; **46**: 2077; Šurca Vuk A, Orel B, Opara Krasovec U, Lavrencic Stangar U, Drazic G. *J. Electrochem. Soc.* 2000; **147**: 2358.
- Delmas C, Cognac-Auraudou H, Cocciantelli JM, Menetrier M, Doumerc JP. *Solid State Ionics* 1994; **69**: 257.

- 1 5. Lu Z, Levi MD, Salitra G, Gofer Y, Levi E, Aurbach D. *J. Electroanal. Chem.* 2000; **491**: 211.
- 2
- 3 6. Aurbach D, Gamolsky K, Markovsky B, Salitra G, Gofer Y, Heider U, Oesten R, Schmidt M. *J. Electrochem. Soc.* 2000; **147**: 1322.
- 4
- 5 7. Alliata D, Koetz R, Haas O, Siegenthaler H. *Langmuir* 1999; **15**: 8483.
- 6
- 7 8. Aurbach D. *J. Power Sources* 2000; **89**: 206.
- 8
- 9 9. Salvi AM, Decker F, Varsano F, Speranza G. *Surf. Interface Anal.* 2001; **31**: 255.
- 10
- 11 10. Levasseur A, Vinatier P, Gonbeau D. *Bull. Mater. Sci.* 1999; **22**: 607; Papageorgopoulos DC, Saltas V, Papageorgopoulos CA, Tonti D, Pettenkofer C, Jaegermann W. *Appl. Surf. Sci.* 2000; **161**: 347; Saltas V, Papageorgopoulos CA, Papageorgopoulos DC, Tonti D, Pettenkofer C, Jaegermann W. *Thin Solid Films* 2001; **389**: 307.
- 12
- 13 11. Jeong JI, Hong JH, Moon JH, Kang J-S. *J. Appl. Phys.* 1996; **79**: 9343.
- 14
- 15 12. Södergren S, Siegbahn H, Rensmo H, Lindström H, Hagfeldt A, Lindquist S-E. *J. Phys. Chem.* 1997; **B 101**: 3087.
- 16
- 17 13. Schechter A, Aurbach D, Cohen H. *Langmuir* 1999; **15**: 3334; Kanamura K, Tamura H, Shiraishi S, Takehara Z. *J. Electroanal. Chem.* 1995; **394**: 49.
- 18
- 19 14. Lourenco A, Masetti E, Decker F. *Electrochim. Acta* 2001; **46**: 2257.
- 20
- 21 Q2 15. Artuso F. *Electrochim. Acta* 2002.●
- 22
- 23 16. Šurca A, Orel B. *Electrochimica Acta* 1999; **44**: 3051.
- 24
- 25 17. Levi MD, Lu Z, Aurbach D. *Solid State Ionics* 2001; **143**: 309.
19. Bisquert J, Garcia-Belmonte G, Bueno P, Longo E, Bulhoes LOS. *J. Electroanal. Chem.* 1998; **452**: 229. 26
20. Aurbach D, Levi MD, Levi E, Teller H, Markovsky B, Salitra G. *J. Electrochem. Soc.* 1998; **145**: 3024; Aurbach D, Markovsky B, Levi MD, Levi E, Schechter A, Moshkovich M, Cohen Y. *J. Power Sources* 1999; **81**: 95. 27
21. Matienzo LJ, Yin LI, Grim SO, Swartz Jr. WE. *Inorg. Chem.* 1973; **12**: 2762. 28
22. Burdese A, Brisi C. *Atti Accad. Sci. Torino* 1961; **95**: 9. 29
23. Castle JE, Salvi AM, Decker F, Moretti G. *Surf. Interface Anal.* 2002.● 30
24. Orel B, Šurca Vuk A, Opara Krasovec U, Drazic G. *Electrochim. Acta* 2001; **46**: 2059. 31
25. Baba Ali E, Bernède JC, Guyomard D. *Thin Solid Films* 2002; **402**: 215. 32
26. McIntyre NS, Cook MG. *Anal. Chem.* 1975; **47**: 2208. 33
27. McIntyre NS, Rummey TE, Cook MG, Owen D. *J. Electrochem. Soc.* 1976; **123**: 1164. 34
28. PF, Luo T, Kuwana DKP, Sherwood PMA. *Anal. Chem.* 1996; **68**: 3330. 35 Q2
29. Wagner CD, Gale LH, Raymond RH. *Anal. Chem.* 1979; **51**: 466. 36
30. Decker F, Artuso F, Cimino N, Zanoni R. IME-5, International Meeting on Electrochromism, Golden, CO, August 2002. 37
31. Connor JA, Hillier IH, Saunders VR. *Mol. Phys.* 1990; **23**: 81. 38
32. Schechter A, Aurbach D, Cohen H. *Langmuir* 1999; **15**: 3334; Zhuang G, Wangand K, Ross Jr PN. *Surf. Sci.* 1997; **387**: 199; Kanamura K, Tamura H, Shiraishiand S, Takehara Z-I. *J. Electroanal. Chem.* 1995; **394**: 49. 39
33. Hoppe H-W, Strehlow H-H. *Surf. Interface Anal.* 1989; **14**: 121. 40
- 41
- 42
- 43
- 44
- 45
- 46
- 47
- 48
- 49
- 50

UNCORRECTED PROOF

1
2
3
4
5
6
7
8
9
10
11
12
13
14
15
16
17
18
19
20
21
22
23
24
25
26
27
28
29
30
31
32
33
34
35
36
37
38
39
40
41
42
43
44
45
46
47
48
49
50
51
52
53
54
55
56
57
58
59
60

QUERIES TO BE ANSWERED BY AUTHOR (SEE MARGINAL MARKS)

IMPORTANT NOTE: Please mark your corrections and answers to these queries directly onto the proof at the relevant place. Do NOT mark your corrections on this query sheet.

Query No.	Query
Q1	RC?
Q2	Vol and page?

61
62
63
64
65
66
67
68
69
70
71
72
73
74
75
76
77
78
79
80
81
82
83
84
85
86
87
88
89
90
91
92
93
94
95
96
97
98
99
100
101
102
103
104
105
106
107
108
109
110
111
112
113
114
115
116
117
118
119
120

UNCORRECTED PROOFS